

Atmospheric-pressure stability of energetic phases of carbon

C. Mailhot and A. K. McMahan

Lawrence Livermore National Laboratory, Livermore, California 94550

(Received 11 April 1991)

The stability of various energetic phases of carbon is investigated with the use of *ab initio* pseudopotential total-energy methods. In particular, we examine the atmospheric-pressure stability of the fourfold-coordinated bc8 phase of carbon against transformations to graphitic and diamond structures lying at lower energy. A group-theoretical analysis is used to determine high-symmetry transformation paths to these low-energy structures. *Ab initio* total-energy calculations are then carried out along those paths characterized by minimal bond breaking to identify minimum-energy configurational transformations. In all cases we find energy barriers inhibiting transformation from the bc8 structure to the lower-energy phases, with the smallest barrier being approximately 0.2 eV/atom and occurring along specific paths to the graphitic forms of carbon. Consequently, it appears that bc8 carbon should be metastable at atmospheric pressure against spontaneous transformation to the lower-energy observed phases. In contrast, we find three metallic high-coordination forms of carbon (face-centered cubic, hexagonal close-packed, and body-centered cubic) to be mechanically unstable against spontaneous transformation to the cubic diamond structure.

I. INTRODUCTION

There has been dramatic progress during the past decade toward the synthetic growth of diamond and diamondlike films using such techniques as plasma discharge and chemical vapor deposition.¹ A recurrent theme in the literature is the possibility that such diamondlike products may contain new crystalline forms of carbon. Among the structures that have been discussed are those referred to as C_8 ,² bc8,³ various 3- and 4-connected nets,^{4,5} $H-6$,^{6,7} and face-centered cubic.⁸

It is the purpose of this paper to examine the mechanical stability⁹ at atmospheric pressure of some of these hypothetical forms of carbon. That is, we seek to determine whether the total energy surface as a function of the atomic coordinates truly has local minima corresponding to such high-energy modifications, or, on the other hand, whether these structures are likely to spontaneously transform to one of the lower-energy observed phases during the course of a lattice vibrational period. Among three- and fourfold coordinated candidate structures we have selected the bc8 phase for investigation, and our results suggest that bc8 carbon is indeed likely to be metastable at atmospheric pressure and low temperature. In contrast, we find the face-centered cubic, hexagonal close-packed, and body-centered cubic structures of carbon to be mechanically unstable at atmospheric pressure in bulk form.

The bc8 structure stands out among other candidate metastable carbon phases for a number of reasons. It is predicted to be the high-pressure stable form of carbon between approximately 1.1 and 2.7 TPa (1 TPa= 10 Mbar).¹⁰⁻¹² A bc8 phase of neighboring group-IV member Si is also experimentally found to be metastable at atmospheric pressure.¹³ Silicon transforms under pres-

sure from its ambient cubic diamond structure to a β -Sn phase, which reverts to a metastable bc8 phase (γ -Si) on decompression.¹⁴ Although structural similarities between members of the same group are common, it should also be emphasized that an important difference from silicon in the present case is the absence of p electrons in the carbon core. Another reason for the particular interest in the bc8 structure is the suggestion,³ based on bond length arguments, that a new cubic form of carbon, apparently synthesized by the condensation of carbon plasmas onto cooled substrates, was really bc8 and not C_8 as the authors claimed.²

Our results for both bc8 carbon and the more closely packed structures reaffirm what may be a general expectation: Any bulk form of carbon, which is metastable at room temperature and atmospheric pressure, is likely to be either threefold (sp^2 bonding) or fourfold (sp^3 bonding) coordinated. First, all well-characterized allotropes of carbon at ambient conditions exhibit such coordinations. These include cubic and hexagonal diamond,¹³ hexagonal and rhombohedral graphite,¹³ and the C_{60} molecular solid.¹⁵ Second, recent *ab initio* molecular dynamics simulations of amorphous carbon, quenched from a disordered liquid state, show only three- and fourfold coordinated sites.¹⁶ Finally, *ab initio* total-energy calculations have so far indicated that structures with higher coordination are mechanically unstable at atmospheric pressure, e.g., sixfold β -Sn and simple cubic.¹² We now add eightfold coordinated body-centered cubic, and 12-fold coordinated face-centered cubic and hexagonal close-packed structures to the list of mechanically unstable phases of carbon at atmospheric pressure.

The expectation that high-coordination forms of carbon are likely to be mechanically unstable in the bulk at atmospheric pressure does not imply the converse, how-

ever. In fact, recent theoretical work indicates that three-fold sp^2 -coordinated H -6 is also mechanically unstable at atmospheric pressure.⁷

The present total-energy calculations have been carried out using *ab initio* pseudopotential methods. We believe this to be the first such effort aimed at addressing the question of the metastability of bc8 carbon at atmospheric pressure. However, equation of state calculations for this phase have been carried out by three groups, all predicting a high-pressure transformation from the ambient diamond phase of carbon to bc8 in the vicinity of 1.1–1.2 TPa as noted above.^{10–12} As a test of our calculations we reproduce these equation of state results and the high-pressure transition in excellent agreement with earlier work.^{10–12}

In principle, one may demonstrate mechanical stability of a given phase by showing that all phonon frequencies are real, which is equivalent to demonstrating a local minimum in the total-energy surface as a function of the atomic coordinates. For a structure such as bc8, with 24 modes at each point in the Brillouin zone, such calculations even at high-symmetry points are challenging to the point of being impractical. They also provide no information about energy barrier heights, a crucial parameter in any investigation of metastable lifetime.

We therefore follow a different approach, motivated by the collective aspect of martensitic transformations. Specifically, we use a symmetry analysis to enumerate all possible transformation paths from the bc8 structure to the lower-energy diamond and graphitic phases which involve 16 or fewer atoms per conventional cell and 6 or more point-group operators. The anticipated energy barriers associated with these paths may be simply ordered according to the number of broken bonds, an ordering which is confirmed by *ab initio* pseudopotential calculations of the barrier heights encountered along selected paths. We then perform detailed *ab initio* pseudopotential total-energy calculations for the paths exhibiting the least amount of bond breaking and identify minimum-energy martensitic transformations from which we extract the barrier height. These calculations strongly suggest, but do not prove in an absolute manner, that bc8 carbon should be mechanically stable at atmospheric pressure, with a barrier height of ≈ 0.2 eV/atom inhibiting its decay to lower-energy graphite phases.

Although our results suggest that bc8 carbon will not spontaneously decay to one of the lower-energy phases at atmospheric pressure, it should be cautioned that the question of whether or not its metastable lifetime is of practical interest lies beyond the scope of the present work. This lifetime is likely to depend on the full topology of the total-energy surface, beyond just the minimum energy barrier discussed here, and will require some form of finite-temperature molecular dynamics simulation for its evaluation. To emphasize this point, note that *ab initio* total-energy calculations have indicated the existence of a 0.33 eV/atom minimum barrier between rhombohedral graphite and cubic diamond, and a slightly larger barrier between a hypothetical $\cdots[AA]\cdots$ -stacked graphite and hexagonal diamond.¹⁷ While perhaps relevant to a shock-induced martensitic

transformation between hexagonal graphite and diamond phases,¹⁸ reaction rates for the graphitization of diamond at high temperatures appear to require an effective barrier height closer to the vaporization energy, or about 7.6 eV/atom.¹⁹ Thus *effective* barrier heights of relevance to thermal stability can in some cases be dramatically larger.

The paper is organized as follows. A detailed symmetry analysis of the various structures and of their transformation into one another is presented in Sec. II. The total-energy method is briefly described in Sec. III. In Sec. IV we present our results for the equation of state of the different phases of carbon and in Sec. V we address the issue of the atmospheric-pressure mechanical stability of these phases. A summary is presented in Sec. VI.

II. SYMMETRY ANALYSIS

There are an infinite number of ways in which one crystalline structure may be deformed into another. Subgroups common to the space groups of both the initial and final structures provide one means of generating such transformation paths in a systematic manner, beginning with those paths of the highest possible symmetry. In this section we use such an analysis to determine high-symmetry paths from the bc8 structure to, what are for solid carbon, lower energy diamond and graphitic structures. The most important paths are discussed here, with more complete symmetry information given in the Appendix, as well as selected paths from various high-coordination structures to cubic diamond.

A given crystal structure may be specified by the space group and site letter(s) as given in the *International Tables for Crystallography*.²⁰ The bc8 structure, for example, is described by space group $Ia\bar{3}$ (T_h^7 , No. 206) with 16 atoms at the c sites (16c) of the conventional or unit cell. There are 8 atoms per *primitive* cell of the body-centered cubic Bravais lattice, leading to the nomenclature “bc8.” The 16c sites of $Ia\bar{3}$ are given by the coordinate triplets

$$\begin{aligned} x, x, x : \quad & \bar{x} + \frac{1}{2}, \bar{x}, x + \frac{1}{2}, \quad \bar{x}, x + \frac{1}{2}, \bar{x} + \frac{1}{2}, \\ & x + \frac{1}{2}, \bar{x} + \frac{1}{2}, \bar{x}, \\ \bar{x}, \bar{x}, \bar{x} : \quad & x + \frac{1}{2}, x, \bar{x} + \frac{1}{2}, \quad x, \bar{x} + \frac{1}{2}, x + \frac{1}{2}, \\ & \bar{x} + \frac{1}{2}, x + \frac{1}{2}, x, \end{aligned} \tag{1}$$

plus the same quantities added to the body center $(\frac{1}{2}, \frac{1}{2}, \frac{1}{2})$. Here, $\bar{x} \equiv -x$. In this paper, following established conventions in crystallography,²⁰ a coordinate triplet (x, y, z) will always be taken to imply the position $x\mathbf{a} + y\mathbf{b} + z\mathbf{c}$, where the vectors \mathbf{a} , \mathbf{b} , and \mathbf{c} define the *conventional* or *unit* cell of the Bravais lattice, and need not be orthogonal. For the cubic system which includes bc8, the three vectors are of course orthogonal and of equal length. Beyond the generic information given by the space group and site letter, values of the lattice constant $a = |\mathbf{a}|$ and of the dimensionless internal parameter x must be specified to give that specific bc8 structure which might, for example, be assumed by carbon at at-

mospheric pressure. At the equilibrium atomic volume, our total-energy calculations indicate that $x_{bc8} = 0.0955$ for such a hypothetical phase of carbon, consistent with the experimental value $x_{bc8} = 0.1003$ for metastable bc8 Si at atmospheric pressure.¹³ These bc8 lattices have slightly distorted tetrahedral coordination, in which one of the bond lengths (between x, x, x and $\bar{x}, \bar{x}, \bar{x}$) is $\approx 4\%$ shorter than the other three.

The *International Tables for Crystallography*²⁰ also list the maximal subgroups contained in each space group. These may reduce the point group while leaving the Bravais lattice unchanged, decenter the conventional cell as in body centered (I) \rightarrow primitive (P), or enlarge the conventional cell as indicated. By tracing subgroups of these subgroups, and so on, one may list all subgroups of the parent space group with, for example, a given number of point-group operators. Cross comparison of such lists for two parent structures may yield common subgroups, which will indicate transition paths between the two structures, *provided* that the site letters also match. We consider transition paths, which are themselves crystal structures, to be of high symmetry when they have relatively large point groups *and* relatively small numbers of atoms per conventional cell.

We find one space group, orthorhombic $Pbca$, to be particularly important among high-symmetry paths from bc8 to the diamond and graphitic structures. The mappings are given in Table I. In addition to the observed allotropes,²¹ cubic diamond (cd), hexagonal diamond (hd), rhombohedral graphite (rg), and hexagonal graphite (hg), we also consider a hypothetical orthorhombic form²² (og) of graphite. As shown in Fig. 1, og rep-

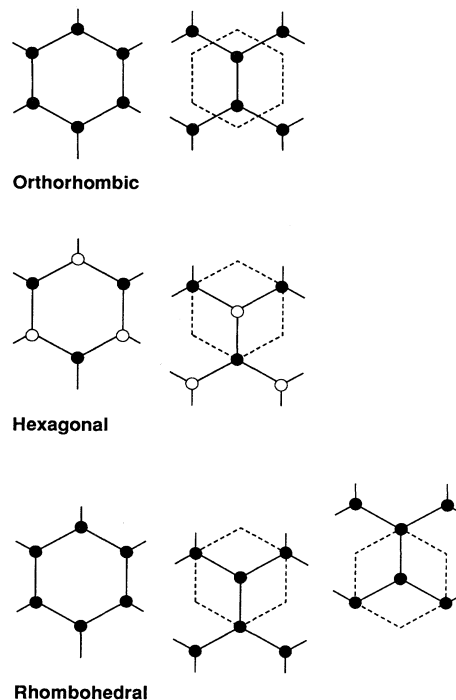


FIG. 1. Graphite structures. The registry of different hexagonal layers in the unit cell is shown relative to the dashed hexagon of the basal plane. Solid and open circles designate inequivalent sites. Only hexagonal and rhombohedral graphite are experimentally observed.

TABLE I. $Pbca$ (D_{2h}^{15} , No. 61) paths from bc8 to hexagonal diamond (hd), cubic diamond (cd), hexagonal graphite (hg), and orthorhombic graphite (og, see Ref. 22). The $Pbca$ conventional cell is primitive orthorhombic with edge lengths a , b , and c . The relations between the $Pbca$ parameters and the usual cubic (a_{bc8} , $x_{bc8} \approx 0.1$, a_{cd}) or hexagonal (a_{hd} , c_{hd} , a_{hg} , c_{hg}) quantities are shown, as well as appropriate $p = 0$ values (a_0 , b_0 , and c_0) of the $Pbca$ lattice constants for carbon. The dimensionless parameters x_1 , y_1 , and z_1 define one set of $8c$ sites; x_2 , y_2 , and z_2 , another. The $8c$ sites are given by $\pm(x, y, z)$, $\pm(\bar{x} + \frac{1}{2}, \bar{y}, z + \frac{1}{2})$, $\pm(\bar{x}, y + \frac{1}{2}, \bar{z} + \frac{1}{2})$, and $\pm(x + \frac{1}{2}, \bar{y} + \frac{1}{2}, \bar{z})$. Note that the bc8 structure may be described *either* by $x_0 = x_{bc8}$ or by $x_0 = \frac{1}{4} - x_{bc8}$. Also note that $Ibca$ (D_{2h}^{27} , No. 71) suffices for the bc8 \rightarrow og path, which does not require decentering.

	bc8	hd	cd	hg	og
a	a_{bc8}	$2 a_{hd}$	$a_{cd}/\sqrt{2}$	$2 a_{hg}$	$2 a_{hg}$
b	a_{bc8}	$\sqrt{3} a_{hd}$	$\sqrt{2} a_{cd}$	$\sqrt{3} a_{hg}$	$\sqrt{3} a_{hg}$
c	a_{bc8}	c_{hd}	$2 a_{cd}$	c_{hg}	c_{hg}
a_0 (Å)	4.42	5.04	2.52	4.92	4.92
b_0 (Å)	4.42	4.37	5.04	4.26	4.26
c_0 (Å)	4.42	4.12	7.13	6.71	6.71
x_1	x_0	$\frac{1}{8}$	$\frac{1}{4}$	$\frac{1}{8}$	$\frac{1}{8}$
y_1	x_0	$\frac{1}{12}$	0	$\frac{3}{12}$	$\frac{1}{6}$
z_1	x_0	$\frac{1}{16}$	$\frac{1}{16}$	$\frac{1}{4}$	$\frac{1}{4}$
$x_2 - \frac{1}{2}$	x_0	$\frac{1}{8}$	$\frac{1}{4}$	$\frac{1}{8}$	$\frac{1}{8}$
$y_2 - \frac{1}{2}$	x_0	$-\frac{1}{12}$	$\frac{1}{4}$	$\frac{1}{12}$	$\frac{1}{6}$
$z_2 - \frac{1}{2}$	x_0	$\frac{1}{16}$	$\frac{5}{16}$	$\frac{1}{4}$	$\frac{1}{4}$

resents a different registry of the hexagonal layers from either of the observed forms of graphite. A monoclinic distortion of the bc8 \rightarrow og path given in Table I will admit rg as the final state (see Appendix). On the energy scale of relevance to this paper, however, all five (cd, hd, rg, hg, and og) phases of carbon may be considered degenerate in total-energy at atmospheric pressure, and equally valid target structures.

To illustrate how Table I provides transformation paths, recall that bc8 is characterized by one lattice constant a and one internal parameter x . The conventional cell in Table I is orthorhombic so that in general a relaxes to $a \neq b \neq c$, and x relaxes to $x \neq y \neq z$. The cell has also been decentered so that the 16c sites of $Ia\bar{3}$ split into two independent sets of 8c sites in $Pbca$. This splitting may occur in two different ways according to whether the bc8 lattice is described by $x_0 = x_{bc8} \approx 0.1$ or by $x_0 = \frac{1}{4} - x_{bc8} \approx 0.15$. The latter choice describes the same bc8 lattice, however, shifted by $-(\frac{1}{4}, \frac{1}{4}, \frac{1}{4})$. It is evident from Table I that both aspects of the symmetry reduction are essential to achieve transformations from bc8 to hd, cd, or hg; although decentering is not required for the og case where body-centered $Ibca$ suffices. To establish a transition path it remains only to define nine continuous functions of a linear transformation variable $a(\xi)$, $b(\xi)$, $c(\xi)$, $x_1(\xi)$, \dots , $z_2(\xi)$ so that for the range $\xi = 0 \rightarrow 1$ these functions evolve from bc8 values to some set of target values.

Two caveats should be mentioned. First, there are 128 ways in which atoms in two 8c sets of one of the structures may be associated with those of another. An obvious choice, which has already been adopted in Table I, is to associate atoms so as to minimize the individual atomic displacements required to achieve the transition. The related issue concerning the choice of x_0 in Table I has already been noted. Second, the lattice constants and perhaps some of the internal coordinates should be determined along the transition path by minimization of the total energy. Such a procedure will be used for the important bc8 \rightarrow og path, and some adjustment will also be made to the bc8 \rightarrow hd path. If the atomic displacements and the associated volume variations are not too large, however, linearized paths may suffice for initial qualitative examinations. We take

$$u = u_{bc8}(1 - \xi) + u_{target}\xi, \quad (2)$$

where $u = a, b, c, x_1, \dots, z_2$, and equilibrium (i.e., zero pressure, $p = 0$) values are used for u_{bc8} and u_{target} .

Metastability of bc8 carbon would require that *all* transition paths to the lower energy diamond and graphitic phases have positive energy barriers. Those paths with potentially the smallest, or perhaps no barriers are thus key to the issue of metastability, and must be investigated by detailed total-energy calculations. Since all of the present structures are sp^2 or sp^3 bonded, such low-barrier paths are likely to be those involving the least amount of bond breaking, and are easily identified. To demonstrate this point, Figs. 2(a) and 2(b) show the four nearest-neighbor distances (bond lengths) along linearized $Ibca$ or $Pbca$ paths from bc8 ($\xi = 0$) to og and hd ($\xi = 1$), respectively. One of these bond lengths is

seen to grow larger during the course of the bc8 \rightarrow og transformation in Fig. 2(a). It is a bond between atoms that will end up in different graphite layers at $\xi = 1$, and is clearly broken during the course of the transformation. Figure 2(a) also describes the bc8 \rightarrow hg transformation, as will be discussed shortly. There are two inequivalent sites along the $Pbca$ path from bc8 to hd, as is evident in Fig. 2(b) by the differing evolutions (dotted versus solid line) of the bc8 short bond. The evolution of the three long bc8 bonds (dash-dot lines) is the same for each site.

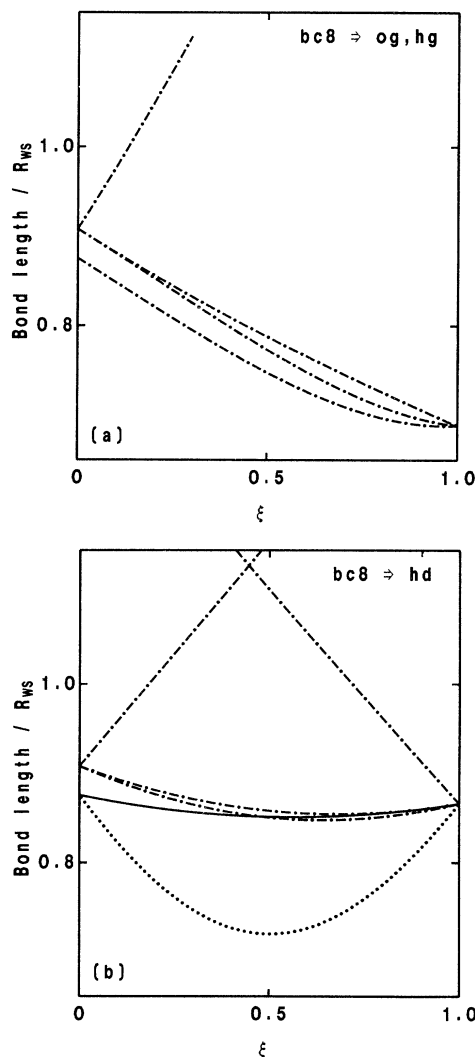


FIG. 2. Bond lengths along linearized transformation paths from bc8 ($\xi = 0$) to og, hg, or hd ($\xi = 1$). (a) The bc8 \rightarrow og (path 1, Table II) and bc8 \rightarrow hg (path 2) mappings yield identical curves for the first three neighbor distances, the fourth differs by only 0.5% at $\xi = 0.3$. (b) Near-neighbor distances to one (solid line), the other (dotted), or both (dash-dot lines) of the two inequivalent 8c sites in the bc8 \rightarrow hd (path 3) mapping. Bond lengths are given relative to the Wigner-Seitz radius R_{ws} along each path.

The crossing of the dash-dot curves at the top of Fig. 2(b) signifies that one of the four near neighbors in hd ($\xi = 1$) was not a near neighbor at the bc8 starting point ($\xi = 0$), i.e., that a bond was broken and then reformed during the transformation. The linearized paths shown in Fig. 2 are entirely adequate for the topological assessment of the number of bonds broken during the transformations, which is for both Figs. 2(a) and 2(b) one bond per atom. In regard to minimum barrier heights; however, our experience reported in Sec. IV suggests that these linearized paths increase c/a too rapidly for the graphitic mappings, and needlessly compress one of the bonds in the mapping to hd.

Table II lists our high-symmetry mappings from bc8 to the diamond and graphitic structures arranged in order of increasing number of broken bonds *per atom*. Fractional values arise when different numbers of bonds are broken on inequivalent sites, e.g., $2c$ and $6f$ of $R\bar{3}$. We believe Table II includes all mappings involving conventional cells of 16 or fewer atoms, and point groups with 6 or more operators, aside from further subgroups of space groups already in the table which might satisfy these conditions.

It is clear that the first three entries in Table II, those paths to og, hg, and hd which break only a single bond per atom, are of greatest interest in regard to the question of possible atmospheric-pressure metastability of bc8 carbon. Henceforth, in referring to $bc8 \rightarrow og$, hg, and hd transformations we shall intend these mappings, unless specifically indicated otherwise. The total energy calculations reported in Sec. IV show the graphitic routes to have the lowest barrier heights, and so we conclude this section with more detailed structural comments on the closely related *Ibca* and *Pbca* paths from bc8 to og and hg, respectively.

The bc8 structure may be viewed as the stacking of double layers along, say, the c direction. Taking $x_{bc8} = 0.1$ for illustrative purposes, there are successive layers of atoms whose c coordinates are

$$(-0.1, 0.1), (0.4, 0.6), (0.9, 1.1), \dots,$$

for $x_0 = x_{bc8}$,

or

$$-0.15, (0.15, 0.35), (0.65, 0.85), 1.15, \dots,$$

$$\text{for } x_0 = \frac{1}{4} - x_{bc8},$$

where the parentheses enclose the double layers. When viewed along the c direction, these double layers resemble a puckered form of the hexagonal layers in graphite as shown in Fig. 3, where the double layers (0.15, 0.35) and (0.65, 0.85) are sketched in Figs. 3(a) and 3(b), respectively. This structure suggests transformation paths in which the double layers are both flattened and pulled apart from one another in the c direction. The simplest path of this kind is the *Ibca* path to og, which was first suggested in the literature without quantitative descriptions.¹² Depending on the choice of x_0 , the target og parameter values are

$$a/b = \sqrt{3}/2, \quad x = \frac{1}{12}, \quad y = \frac{1}{8}, \quad z = 0,$$

$$\text{for } x_0 = x_{bc8},$$

or

$$a/b = 2/\sqrt{3}, \quad x = \frac{1}{8}, \quad y = \frac{1}{6}, \quad z = \frac{1}{4},$$

$$\text{for } x_0 = \frac{1}{4} - x_{bc8}.$$

The atoms starting at (x_0, x_0, x_0) and at $(-x_0, -x_0, -x_0)$ should end up in the same hexagonal layers for $x_0 = x_{bc8}$, so that the target value of z is $z = 0$; while for $x_0 = \frac{1}{4} - x_{bc8}$, they should end up in different layers, so the target value is $z = \frac{1}{4}$. The former representation is more easily visualized and has been adopted in the Appendix when describing a monoclinic distortion of the $bc8 \rightarrow og$ path. The latter is adopted in Table I to permit more natural comparisons between the og and hg paths.

The two choices of origin for the $bc8 \rightarrow og$ mapping are taken at centers of inversion which lie in the first case *within* the double or hexagonal layers, and in the second case, *between* these layers. Only the second choice is

TABLE II. Bonds broken (per atom) in high-symmetry mappings from bc8 to diamond and graphitic structures. The choice of x_0 is relevant only to the *Pbca/Ibca* paths indicated in Table I.

Path	Target structure	x_0	Space group	Sites	Bonds broken
1	Orthorhombic graphite	$\frac{1}{4} - x_{bc8}$	<i>Ibca</i>	16 <i>f</i>	1.0
2	Hexagonal graphite	$\frac{1}{4} - x_{bc8}$	<i>Pbca</i>	8 <i>c</i> , 8 <i>c</i>	1.0
3	Hexagonal diamond	x_{bc8}	<i>Pbca</i>	8 <i>c</i> , 8 <i>c</i>	1.0
4	Cubic diamond		$R\bar{3}$	2 <i>c</i> , 6 <i>f</i>	1.5
5	Rhombohedral graphite		$R\bar{3}$	2 <i>c</i> , 6 <i>f</i>	1.75
6	Orthorhombic graphite	x_{bc8}	<i>Ibca</i>	16 <i>f</i>	2.0
7	Hexagonal graphite	x_{bc8}	<i>Pbca</i>	8 <i>c</i> , 8 <i>c</i>	2.0
8	Hexagonal diamond	$\frac{1}{4} - x_{bc8}$	<i>Pbca</i>	8 <i>c</i> , 8 <i>c</i>	2.0
9	Cubic diamond	$\frac{1}{4} - x_{bc8}$	<i>Pbca</i>	8 <i>c</i> , 8 <i>c</i>	2.0
10	Hexagonal diamond		<i>Pcca</i>	8 <i>f</i> , 8 <i>f</i>	2.0
11	Cubic diamond	x_{bc8}	<i>Pbca</i>	8 <i>c</i> , 8 <i>c</i>	2.5

possible for the $bc8 \rightarrow hg$ mapping, as hg has inversion symmetry only at points in between its hexagonal layers. A comparison of the og and hg target values in Table I shows differences only in the y values, $y_1 = y_2 - \frac{1}{2} = \frac{1}{6}$ for og , and $y_1 = \frac{3}{12}$, $y_2 - \frac{1}{2} = \frac{1}{12}$ for hg . All atoms remain equivalent along the former path (thus $1bca$), while two inequivalent $8c$ sets evolve along the latter, as required by the two inequivalent sites in the hg structure. Nevertheless, linear mappings using the parameters in the table yield nearly identical near-neighbor environments for the two cases, with only more distant neighbors introducing the inequivalency in the hg case. As noted in Fig. 2(a), distances to the first three neighbors are identical for the two paths at all stages of the transformation, while that

to the fourth is only 0.5% different by $\xi = 0.3$. Since the total energy for covalent carbon is completely dominated by near-neighbor interactions, as may be judged, for example, from essentially identical equations of state for cd and hd , we need investigate only one of the two graphitic paths. The $bc8 \rightarrow og$ path is the obvious choice because of the reduced computational expense following from its smaller number of atoms per primitive cell.

III. THEORETICAL TOTAL-ENERGY METHOD

The results presented below were obtained using *ab initio* pseudopotentials implemented with a plane-wave basis for the expansion of the electronic wave functions. These pseudopotential calculations are performed within the framework of local density-functional theory²³ applied in the momentum-space formalism.²⁴ We use non-local, norm-conserving,²⁵ *ab initio* ionic pseudopotentials as tabulated by Bachelet *et al.*²⁶ The Ceperley-Alder²⁷ model is used for the exchange-correlation potential. In addition to the total energy E , the stress tensor, the pressure p , the enthalpy $H = E + pV$, and the forces are calculated analytically from the stress theorem.²⁸ Brillouin zone summations are performed using sets of special \mathbf{k} points generated using the Monkhorst-Pack algorithm.²⁹ Details of the computational procedure have been documented in the literature.³⁰

Carbon is an element for which a pseudopotential description should be adequate because the core $1s^2$ states do not overlap significantly with the valence states. However, since the core of carbon consists only of $1s^2$ states, there is no cancellation for the p and d states in the core region and, consequently, the resulting pseudopotentials are very attractive for these angular momentum channels. As a result, a large number of plane waves are required to provide a correct description of the carbon pseudofunction.

IV. EQUATION OF STATE

In this section we report results of our pseudopotential calculations for the ground-state properties of various phases of carbon. We first present equations of state for the eight structures considered in this study, and tabulate their ground-state properties and total-energy differences between these phases at their equilibrium (i.e., $p = 0$) volumes. Most of the crystal structures considered below are well known, and their description may be found elsewhere.¹³ In addition, the $bc8$ structure has been discussed at some length in Sec. II, and a description of the orthorhombic graphite structure is provided in Ref. 22 and is illustrated in Fig. 1.

The hexagonal diamond phase may be somewhat less familiar and we now provide a brief description of its structure. The hexagonal diamond structure consists of a set of buckled hexagonal rings of atoms stacked in a $\dots[AB]\dots$ sequence along the c direction, while the most abundant cubic diamond structure consists of a set of buckled hexagonal rings of atoms stacked in a $\dots[ABC]\dots$ sequence along the $[111]$ direction.

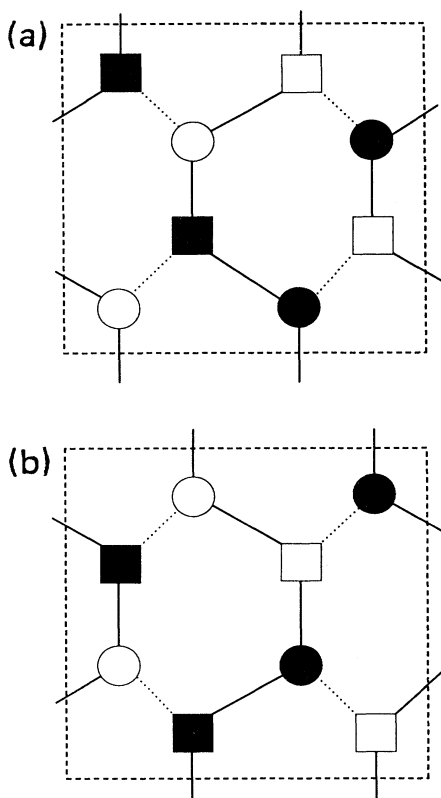


FIG. 3. Projections of the two double layers in the $bc8$ structure. Boundaries of the conventional 16-atom cell in the a,b plane are indicated by dashed lines. Cross sections at $\frac{1}{4}c$ and $\frac{3}{4}c$ are given in (a) and (b), respectively. Sites located $x_{bc8a} \approx 0.1a$ above (below) the indicated cross-sectional planes are represented by solid (open) symbols. Long bonds between near-neighbor atoms are denoted by solid lines; short bonds, by dotted lines. The centers of the short bonds lie exactly over one another in the two cross sections. The $x_0 = \frac{1}{4} - x_{bc8} \approx 0.15$ description (see Table I) of the $bc8$ structure has been assumed, with circles and squares showing the two different sets of $8c$ sites in a $Pbca$ representation. For this description, all four near neighbors of a given atom belong to the other $8c$ set.

The hexagonal diamond structure is characterized by a hexagonal unit cell with a four-atom basis at positions $\pm[\frac{1}{3}(\mathbf{a} + \mathbf{b}) + z\mathbf{c}]$ and $\pm[\frac{1}{3}(\mathbf{a} + \mathbf{b}) + (\frac{1}{2} - z)\mathbf{c}]$, where the angle between the lattice translation vectors \mathbf{a} and \mathbf{b} in the basal planes is equal to $\pi/3$ and \mathbf{c} is perpendicular to the basal plane. Perfect tetrahedral coordination of nearest neighbors is obtained for $c_{hd}/a_{hd} = \sqrt{8/3}$ and $z = \frac{1}{16}$, although these parameters are free and do not alter the crystallographic symmetry.¹³

The results of our *ab initio* plane-wave pseudopotential calculations are indicated in Fig. 4 where the calculated total energy is plotted as a function of atomic volume for the cubic diamond (cd), hexagonal diamond (hd), bc8, orthorhombic graphite (og), simple cubic (sc), body-centered cubic (bcc), hexagonal close-packed (hcp), and face-centered cubic (fcc). Inspection of Fig. 4 reveals an interesting characteristic of the equation of state of carbon: The high-coordination phases have a larger equilibrium volume (i.e., a lower density) than the low-energy fourfold-coordinated phases. This observation is at variance with the equation of state of neighboring group-IV member Si where the density is predicted to increase with increasing coordination number.³¹

All calculations whose results are shown in Fig. 4 were performed with a kinetic energy cutoff of $E_{\text{cutoff}} = 45$ Ry, using Monkhorst-Pack special \mathbf{k} points.³² The corresponding values of the equilibrium energy E_0 , equilibrium atomic volume V_0 , and bulk modulus B_0 are indicated in Table III for the various structures studied. For the cd and og structures, results obtained using various kinetic energy cutoffs are given to indicate the level of convergence of the calculation. The values indicated

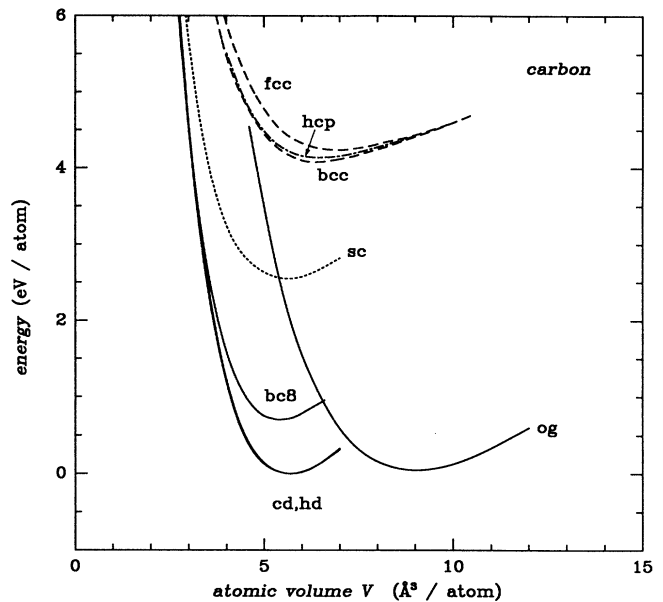


FIG. 4. Calculated total energy per atom as a function of atomic volume for the cubic diamond (cd—solid line), hexagonal diamond (hd—solid line), bc8 (solid line), orthorhombic graphite (og—solid line), simple cubic (sc—dotted line), body-centered cubic (bcc—dashed line), hexagonal close-packed (hcp—dash-dot line), and face-centered cubic (fcc—dashed line). All calculations were performed with a kinetic energy cutoff of $E_{\text{cutoff}} = 45$ Ry. The number of Monkhorst-Pack special \mathbf{k} points used are 10 (cd), 12 (hd), 18 (bc8), 32 (og), 35 (sc), 26 (bcc), 36 (hcp), and 28 (fcc).

TABLE III. Ground-state properties of carbon for the cubic diamond (cd), hexagonal diamond (hd), bc8, simple cubic (sc), body-centered cubic (bcc), hexagonal close-packed (hcp), face-centered cubic (fcc), and orthorhombic graphite (og) structures. For the cd and og structures, results obtained using various kinetic energy cutoffs are given for comparison. The values of the equilibrium atomic volume V_0 , bulk modulus B_0 , and equilibrium energy E_0 with respect to cd are obtained by fitting the calculated total energies to Murnaghan's equation of state (Ref. 33). Available experimental values are given for comparison.

Structure	c/a	$V_0(\text{\AA}^3)$		$B_0(\text{GPa})$		$E_0(\text{eV/atom})$
		Predicted	Observed (Ref. 13)	Predicted	Observed (Ref. 38)	
cd (45 Ry)		5.65	5.67	449	443	0.00
cd (65 Ry)		5.67		441		
cd (90 Ry)		5.49		452		
cd (120 Ry)		5.49		457		
hd (45 Ry)	$\sqrt{8/3}$	5.67	5.67	448		0.002
bc8 (45 Ry)		5.39		454		0.70
sc (45 Ry)		5.56		309		2.56
bcc (45 Ry)		6.63		221		4.08
hcp (45 Ry)	$\sqrt{8/3}$	6.67		168		4.14
fcc (45 Ry)		7.01		233		4.23
og (45 Ry)	2.7259	9.15		271		0.045
og (65 Ry)	2.7259	8.69		263		0.032

in Table III are obtained by fitting the calculated total energies to Murnaghan's equation of state³³

$$E_{\text{total}}(V) = E_0 + \left(\frac{B_0 V}{B'_0} \right) \left(\frac{(V_0/V)^{B'_0}}{B'_0 - 1} + 1 \right). \quad (3)$$

For each crystal structure, the fits to Murnaghan's equation of state were performed using several values of the total energy calculated for lattice constants near the equilibrium volume. For all the fits, the rms errors were typically smaller than 10^{-4} eV/atom.

For the bc8 structure, the internal parameter x describing the positions of the atoms within the bcc primitive cell was optimized for several atomic volumes in the range $2 \text{ \AA}^3 \leq V \leq 6 \text{ \AA}^3$ by calculating the value of x which produces a vanishing force on the atoms. Our results indicate that the variation of the internal parameter x for the bc8 structure in this volume range can be well described by the linear relation

$$x_{\text{bc8}}(V) = x_0 - b(V - 2), \quad (4)$$

where $x_0 = 0.1059$, $b = 3.065 \times 10^{-3} \text{ \AA}^{-3}$, and V is the atomic volume in \AA^3 .

For the og structure,²² the results shown in Fig. 4 were obtained with a value $c_{\text{og}}/a_{\text{og}} = 2.7259$ which corresponds to the experimentally observed value of $c_{\text{hg}}/a_{\text{hg}}$ for hg.¹³ We have explicitly verified the insensitivity of the total energy on the value of the ratio $c_{\text{og}}/a_{\text{og}}$ by performing several calculations of the total energy as a function of atomic volume for various values of the ratio $c_{\text{og}}/a_{\text{og}}$ between 2.50 and 2.80. A least-squares fit analysis of the resulting minimum energy as a function of the value of $c_{\text{og}}/a_{\text{og}}$ reveals that the total energy at equilibrium volume varies by less than 3 meV/atom when the ratio $c_{\text{og}}/a_{\text{og}}$ is varied by ± 0.1 around the minimum value $c_{\text{og}}/a_{\text{og}} \approx 2.74$.

Total-energy calculations of the og structure performed for a kinetic energy cutoff of 45 Ry (65 Ry) indicate that og is unbound with respect to cd by 45 meV/atom (32 meV/atom) at equilibrium. Inclusion of the zero-point motion of the ions at $T = 0$ K reduces this energy difference to 30 meV/atom (17 meV/atom). This result is somewhat at variance with experimental observations which indicate that hg is bound with respect to cd by 27 meV/atom.¹¹ However, a direct comparison of our results with available experimental measurements is somewhat difficult in this case since the stacking of the hexagonal layers in og differs from that in hg. Moreover, our numerical result that og is slightly unbound with respect to cd is not significant within the context of the present study and bears no consequence on the discussion regarding the mechanical stability of the energetic phases of carbon considered below.

The results shown in Fig. 4 for the hd phase were obtained for a structure characterized by perfect tetrahedral coordination, i.e., a ratio $c_{\text{hd}}/a_{\text{hd}} = \sqrt{8/3}$ and an internal parameter $z = \frac{1}{16}$.¹³ For these particular values of $c_{\text{hd}}/a_{\text{hd}}$ and z , the hd and cd structures exhibit identical first neighbor environments, i.e., perfect sp^3 tetrahedral coordinations with ideal bond angles $\theta = \arccos(-\frac{1}{3}) = 109.47^\circ$. Consequently, the ground-

state properties of the cd and hd structures are, not surprisingly, almost identical as an inspection of Table III reveals. The results shown in Fig. 4 for the hcp phase were also obtained for an ideal ratio $c_{\text{hcp}}/a_{\text{hcp}} = \sqrt{8/3}$.

The equilibrium energy per atom E_0 relative to the cd phase is indicated in Table III for the eight structures studied. The equation of state corresponding to the various phases of carbon can be approximately divided into three rather distinct regions well separated in energy and populated by groups of structures exhibiting similar coordination: First, the threefold-coordinated graphitic and fourfold-coordinated diamond and bc8 phases are grouped in a low-energy region. At the equilibrium volume, the energy of the bc8 structure is higher than that of cd by $E_{\text{bc8}} = 0.70$ eV/atom. Second, at approximately 2.5 eV/atom above the cd structure lie the sixfold coordinated phases: sc and β -Sn¹² (the β -Sn phase is not shown in Fig. 4). Third, at approximately 4.0 eV/atom above the cd structure, a high-energy region is populated by phases whose coordination number exceeds six: the eightfold coordinated bcc and the 12-fold coordinated hcp and fcc phases.

From the calculated equation of state shown in Fig. 4, one deduces that a cd \rightarrow bc8 phase transformation is predicted to occur at a pressure of $p_{\text{tr}} = 1.1$ TPa = 11 Mbar. The value of the transition pressure was obtained by equating the enthalpies of the bc8 and cd structures:

$$H_{\text{bc8}} = H_{\text{cd}}, \quad (5)$$

$$E_{\text{bc8}} + p_{\text{tr}} V_{\text{bc8}} = E_{\text{cd}} + p_{\text{tr}} V_{\text{cd}}. \quad (6)$$

This value of the transition pressure is in good agreement with previous calculations which have appeared in the literature¹⁰⁻¹² and range from $p_{\text{tr}} = 1.11$ to 1.2 TPa. Our results also indicate that a subsequent bc8 \rightarrow sc phase transformation is predicted to occur at a pressure of approximately $p_{\text{tr}} = 2.7$ TPa, in excellent agreement with previously reported results.¹¹ However, while stable at high pressure, the sc phase of carbon has been predicted to be mechanically unstable at $p = 0$.¹²

V. ATMOSPHERIC-PRESSURE STABILITY OF PHASES OF CARBON

In this section we present results of our *ab initio* plane-wave pseudopotential calculations on the atmospheric-pressure ($p = 0$) stability of various phases of carbon. We first consider the stability of the fourfold-coordinated bc8 structure against a transformation to lower-energy graphitic and diamond phases. We then consider the stability of the high-coordination phases of carbon.

A. Atmospheric-pressure stability of bc8 carbon

Since the energy of the bc8 structure lies 0.7 eV/atom above the essentially degenerate diamond and graphitic structures, we must consider transformation paths to all of these lower-energy phases as possible sources of mechanical instability in a $p = 0$ bc8 carbon phase. The discussion presented in Sec. II was based on symmetry

and geometrical considerations to identify those paths involving the least amount of bond breaking, and therefore those most likely to exhibit the smallest energy barriers. Extensive total-energy calculations are carried out along these paths to identify minimum-energy configurational transformations between two given phases. We first discuss the $Ibca$ $bc8 \rightarrow og$ mapping (path 1 in Table II), which as noted earlier is essentially identical in regard to near-neighbor environment to the $Pbca$ $bc8 \rightarrow hg$ mapping (path 2), which therefore need not be separately investigated. We subsequently discuss our results for the $Pbca$ $bc8 \rightarrow hd$ mapping (path 3). In addition, so as to substantiate the geometric bond-breaking considerations which lead to the results in Table II, we also consider the very highest energy mapping in Table II to cd (path 11) which also occurs within the $Pbca$ space group.

1. Transformation from $bc8$ to orthorhombic graphite

The $bc8 \rightarrow og$ transformation can be viewed as a two-step process: First the buckling characterizing the $bc8$ double layers is removed as the b/a ratio of the body-centered orthorhombic cell is decreased and subsequently the c/a ratio is increased, resulting in an increase of the interlayer separation. This transformation is schematically indicated in Fig. 5.

The final og structure exhibits a $\cdots[AB]\cdots$ sequence along the c axis, but does not correspond to the hg structure. However, a sliding of the hexagonal planes relative to one another would transform our final og structure into rg . We also examine such a transformation at the end of this section.

The $bc8 \rightarrow og$ transformation has been described in Sec. II. We define a linear transformation variable ξ which continuously transforms the structure from the $bc8$ phase ($\xi = 0$) to the og phase ($\xi = 1$). Along the $bc8 \rightarrow og$ transformation, the total energy is minimized and a minimum-energy surface E_{\min} is mapped. This is accomplished in the following way: For each value of the transformation

parameter ξ , the parameters a , b , and c describing the orthorhombic primitive cell are varied independently so as to minimize the total energy. Only the internal parameters x , y , and z were linearized as a function of ξ . Consequently, our calculations correspond to a constant zero-pressure transformation path.

The results of our calculations for the $bc8 \rightarrow og$ transformation are indicated in Fig. 6(a) where the minimum energy E_{\min} is shown as a function of the configurational variable ξ . Throughout the $bc8 \rightarrow og$ transformation, the structures are described by a primitive cell with an 8-atom basis. The $bc8 \rightarrow og$ transformation involves a large increase in the value of the atomic volume, from $V_{bc8}^{\text{initial}} = 5.39 \text{ \AA}^3$ to $V_{og}^{\text{final}} = 9.15 \text{ \AA}^3$. The final og structure is characterized by an in-plane bond length of $d_{og} = 1.45 \text{ \AA}$ which is in good correspondence with that of the observed hg structure, $d_{hg}^{\text{expt}} = 1.42 \text{ \AA}$.¹³

A kinetic energy cutoff of $E_{\text{cutoff}} = 35 \text{ Ry}$ and 17 special \mathbf{k} points were used for all the calculations along the $bc8 \rightarrow og$ transformation. However, the convergence of our results with respect to kinetic energy cutoff was explicitly verified by performing the energy-minimization procedure described above using a kinetic energy cutoff of $E_{\text{cutoff}} = 45 \text{ Ry}$. The results of these calculations at $E_{\text{cutoff}} = 45 \text{ Ry}$ are also indicated in Fig. 6(a) for $\xi \leq 0.60$, above which the required number of plane waves exceeds our current computing resources. Inspection of Fig. 6(a) reveals the existence of an energy barrier of $\Delta E_b(bc8 \rightarrow og) \approx 0.20 \text{ eV/atom}$ along the $bc8 \rightarrow og$ transformation path. As a result, it appears that the $bc8$ structure is mechanically stable against a transformation toward an og structure.

The energy difference between the initial $bc8$ structure and the final og structure is 0.548 eV , which is less than the equilibrium energy difference between the $bc8$ and og structures indicated by the equation of state Fig. 4 ($\approx 0.655 \text{ eV/atom}$). This discrepancy likely results from the utilization of a smaller energy kinetic energy cutoff ($E_{\text{cutoff}} = 35 \text{ Ry}$) for the calculations whose results are

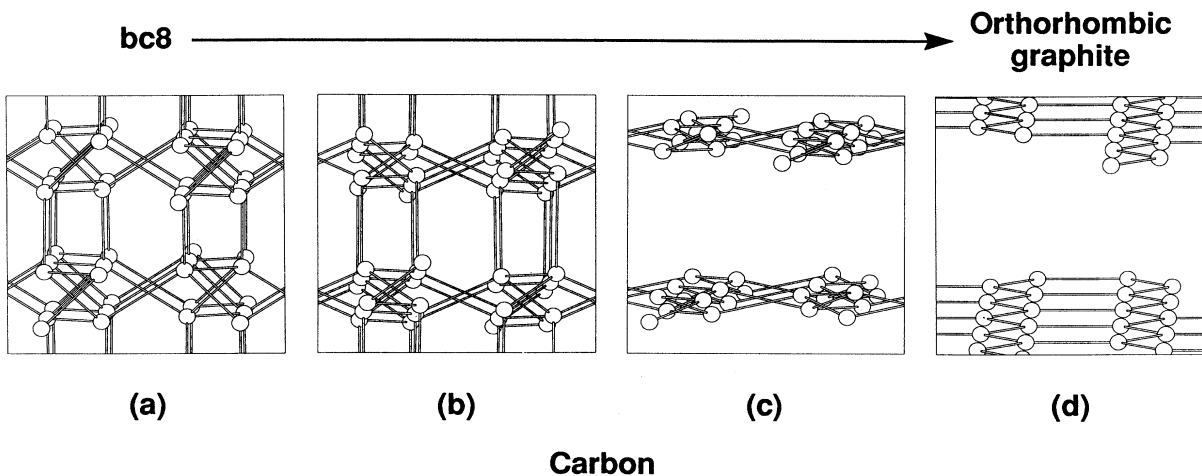


FIG. 5. Schematic indication of the $bc8 \rightarrow og$ transformation (path 1 in Table II). The minimum-energy structure corresponding to the value of the transformation parameter ξ are shown for $\xi = 0$, $\xi = 0.3$, $\xi = 0.7$, and $\xi = 1$ in panels (a), (b), (c), and (d), respectively.

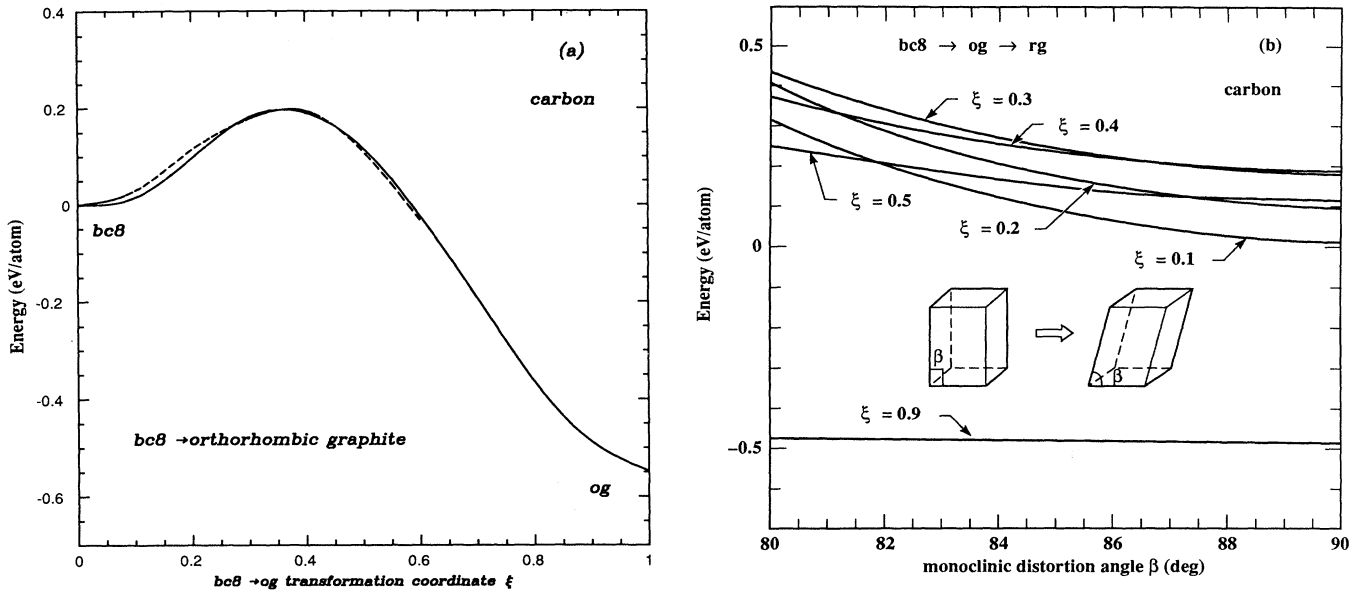


FIG. 6. (a) Calculated total energy per atom as a function of the parameter ξ describing the $bc8 \rightarrow og$ transformation (path 1, Table II). The $bc8$ structure corresponds to $\xi = 0$ and the og structure corresponds to $\xi = 1$. Throughout the $bc8 \rightarrow og$ transformation, the structures are described by a primitive cell with an 8-atom basis. Only the internal parameters x , y , and z were linearized as a function of ξ . The energy was minimized at each ξ with respect to the $Ibca$ lattice constants a , b , and c to yield a constant-pressure ($p = 0$) path. The atomic volume varies along the transformation path from $V_{bc8}^{initial} = 5.39 \text{ \AA}^3$ to $V_{og}^{final} = 9.15 \text{ \AA}^3$. Kinetic energy cutoffs of $E_{cutoff} = 35 \text{ Ry}$ (solid line) and $E_{cutoff} = 45 \text{ Ry}$ (dashed line) and 17 special \mathbf{k} points were used for all the calculations. (b) Calculated energy per atom as a function of the monoclinic angle β for various values of the parameter ξ characterizing the $bc8 \rightarrow og$ transformation. The orthorhombic cell is recovered for the case where $\beta = 90^\circ$. A kinetic energy cutoff of $E_{cutoff} = 35 \text{ Ry}$ and 22 special \mathbf{k} points were used for all the calculations. The zero of energy corresponds to the $bc8$ structure.

shown in Fig. 6(a) than for the calculations of the equation of state indicated in Fig. 4 ($E_{cutoff} = 45 \text{ Ry}$). This discrepancy bears no consequence on our conclusions regarding the mechanical stability of $bc8$ carbon, however, and, as indicated above and shown in Fig. 6(a), convergence studies up to $\xi = 0.60$ reveal that the energy barrier height remains unchanged when the kinetic energy cutoff is increased from $E_{cutoff} = 35 \text{ Ry}$ to $E_{cutoff} = 45 \text{ Ry}$. The utilization of kinetic energy cutoffs exceeding $E_{cutoff} = 35 \text{ Ry}$ are not possible for large atomic volumes [i.e., near the og limit in Fig. 6(a)] with our current computer resources when the og structure is described by an 8-atom basis.

The og structure examined above can be transformed into rg by sliding the og planes relative to each other. This may be achieved by allowing the angle β between the a and c axes of the 16-atom unit cell to differ from 90° , which results in a lowering of the orthorhombic $Ibca$ symmetry to monoclinic $C2/c$. The corresponding mapping is given in the Appendix, and permits a direct $bc8 \rightarrow rg$ transition, or an examination of the energetics of sliding the puckered double layers relative to one another at any stage during the $bc8 \rightarrow og$ mapping.

The results of our total-energy calculations for this sliding of the puckered graphitic layers is shown in Fig. 6(b) where the total energy is plotted as a function of the monoclinic angle β for various values of the parameter ξ characterizing the $bc8 \rightarrow og$ transformation [cf.

Fig. 6(a)]. The $bc8$ structure corresponds to $\xi = 0$ and the og structure corresponds to $\xi = 1$. A kinetic energy cutoff of $E_{cutoff} = 35 \text{ Ry}$ and 22 special \mathbf{k} points were used for all the calculations. Inspection of Fig. 6(b) reveals an increase in total energy as the planes are shifted with respect to one another. Consequently, the structure appears to be stable against a monoclinic distortion of the cell along the $bc8 \rightarrow og$ transformation indicated in Fig. 6(a). Therefore, the $bc8$ structure appears to be metastable against a transformation toward an rg structure, at least prior to complete flattening of the puckered double layers. The results indicated in Fig. 6(b) reveal that close to the planar og structure ($\xi = 0.90$), the total energy is very insensitive to a sliding motion of the planes relative to one another, as expected, since the interaction between the layers is characterized by weak van der Waals forces.

2. Transformations from $bc8$ to cubic and hexagonal diamond

We now consider the energetics associated with the $bc8 \rightarrow cd$ and $bc8 \rightarrow hd$ transformations. The discussion given in Sec. II indicates that the degree of bond-breaking and rebonding is quite severe for the $bc8 \rightarrow cd$ path given as the last entry in Table II, intuitively suggesting a very large energy barrier inhibiting this transformation. The

Pbca bc8 \rightarrow hd mapping (path 3 in Table II), in contrast, requires breaking only one bond per atom, similar to the og path discussed above. One might expect a similar barrier, although probably larger given the significant compression seen in half of the short bonds in Fig. 2(b).³⁴ In order to verify these expectations we have performed calculations of the energetics associated with the bc8 \rightarrow cd and bc8 \rightarrow hd transformations. As in the case discussed in the previous section we consider a linear transformation which maps the bc8 structure onto the cubic and hexagonal diamond phases. Unlike the case of the bc8 \rightarrow og transformation, the atomic geometry is not fully optimized (i.e., the total energy is not minimized) at each configuration point along the linear transformation for the bc8 \rightarrow cd transformation. However, limited minimum-energy atomic configuration searches were performed for the bc8 \rightarrow hd transformation by optimizing the c/a ratio along the transformation mapping. Consequently, the calculations presented in this section correspond only to an approximately zero-pressure ($p \approx 0$) transformation. We believe this procedure to be accurate enough to provide qualitative information on the stability of bc8 carbon since the atomic volume variations characterizing the bc8 \rightarrow cd and bc8 \rightarrow hd transformations are very small (see below). We estimate that the uncertainty in the calculated energy arising from not using the $p = 0$ volumes for the bc8 \rightarrow cd transformation and performing only an optimization of the c/a ratio for the bc8 \rightarrow hd transformation is less than 0.1 eV/atom.

The results of our calculations showing the energy per atom along the transformation path associated with the bc8 \rightarrow cd and bc8 \rightarrow hd transformations are shown in Fig. 7. Throughout the bc8 \rightarrow cd and bc8 \rightarrow hd transformations, the structures are described by a primitive cell with a 16-atom basis. The bc8 \rightarrow cd and bc8 \rightarrow hd transformations both involve a small increase in the value of the atomic volume: from $V_{bc8}^{initial} = 5.39 \text{ \AA}^3$ to $V_{cd}^{final} = 5.65 \text{ \AA}^3$ and $V_{hd}^{final} = 5.67 \text{ \AA}^3$. A kinetic energy cutoff of $E_{cutoff} = 30 \text{ Ry}$ and 8 special \mathbf{k} points were used for all the calculations. Inspection of Fig. 7 reveals the existence of an energy barrier of $\Delta E_b(\text{bc8} \rightarrow \text{hd}) \approx 0.5 \text{ eV/atom}$ along the bc8 \rightarrow hd³⁴ and of an energy barrier of $\Delta E_b(\text{bc8} \rightarrow \text{cd}) \approx 2.0 \text{ eV/atom}$ along the bc8 \rightarrow cd. Comparison between Figs. 6(a) and 7 supports the qualitative argument of Sec. II in which the number of broken bonds associated with different transformations can be used to deduce general results on the relative energy barriers corresponding to these transformations.

The results presented in this section suggest that fourfold-coordinated bc8 carbon would be mechanically stable at atmospheric pressure against a transformation to a lower-energy graphitic or diamond phase. In this respect, bc8 carbon would behave similarly to bc8 Si which is experimentally observed to be mechanically stable at atmospheric pressure when recovered from the high-pressure β -Sn phase. The energy barriers found for the transformations from bc8 carbon are ordered in accordance with simple arguments based on the number of broken bonds for each transformation: $\Delta E_b(\text{bc8} \rightarrow \text{og}) < \Delta E_b(\text{bc8} \rightarrow \text{hd}) < \Delta E_b(\text{bc8} \rightarrow \text{cd})$.

B. Atmospheric-pressure stability of high-coordination metallic phases of carbon

Having presented results which suggest the atmospheric-pressure metastability of fourfold-coordinated bc8 carbon, we now consider the stability of high-energy phases of carbon in which the coordination exceeds four. This determination of the mechanical stability of high-coordination phases of carbon is interesting on the basis of a comparison with neighboring group-IV member Si which, in the liquid state, is experimentally observed to exhibit an average coordination between 6 and 7.^{35,36} Moreover, sixfold and tenfold Si clusters have been predicted to be particularly stable.³⁷

It has already been reported in the literature that the sixfold-coordinated simple cubic and β -Sn phases of carbon were mechanically unstable (i.e., without the existence of an energy barrier) against a transformation to the lower-energy cubic diamond structure.¹² In this section we also consider the stability of the fcc (12-fold coordinated), hcp (12-fold coordinated), and bcc (8-fold coordinated) phases against a transformation to the lower-

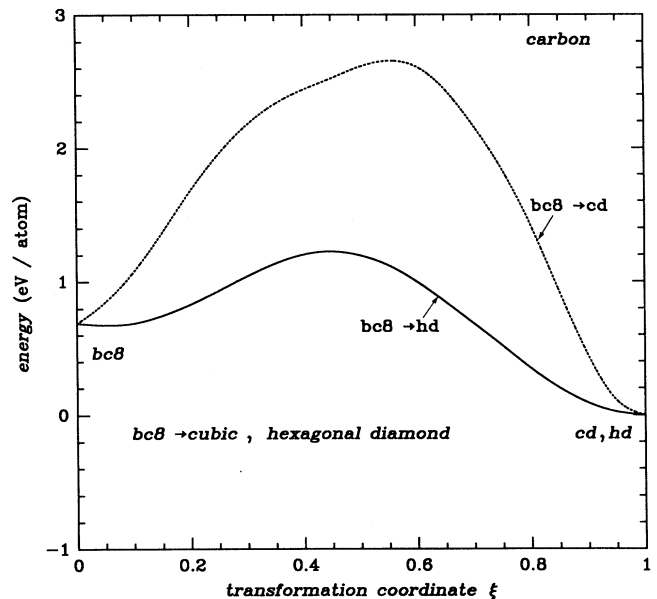


FIG. 7. Calculated total energy per atom as a function of the parameter ξ describing the bc8 \rightarrow cd (path 11, Table II) and bc8 \rightarrow hd (path 3, Table II) transformations. The bc8 structure corresponds to $\xi = 0$ and the value $\xi = 1$ corresponds to the cd or hd phases. Throughout the bc8 \rightarrow cd and bc8 \rightarrow hd transformations, the structures are described by a primitive cell with a 16-atom basis. The calculations correspond to an approximately constant-pressure ($p \approx 0$) path and the atomic volume varies along the transformation path from $V_{bc8}^{initial} = 5.39 \text{ \AA}^3$ to $V_{cd}^{final} = 5.65 \text{ \AA}^3$ and $V_{hd}^{final} = 5.67 \text{ \AA}^3$. A kinetic energy cutoff of $E_{cutoff} = 30 \text{ Ry}$ and 8 special \mathbf{k} points were used for all the calculations. The zero of energy corresponds to the bc8 structure.

energy cd structure. Transformation paths are identified in the Appendix which in each case evolve four of the original 12 or 8 near neighbors in these structures into the four near neighbors of cd. The fcc and hcp transformations are described with four-atom conventional cells in space group $Pnma$; the bcc transformation, with a two-atom cell in space group $R\bar{3}m$.

The results of our calculations are shown in Fig. 8 where the calculated energy per atom is indicated as a function of the parameter ξ describing the following transformations: fcc \rightarrow cd, hcp \rightarrow cd, and bcc \rightarrow cd. Throughout the linear transformations, the structures are described by a primitive cell with a 4-atom basis for the fcc \rightarrow cd and hcp \rightarrow cd transformations and a 2-atom basis for the bcc \rightarrow cd transformation. The fcc \rightarrow cd, hcp \rightarrow cd and bcc \rightarrow cd transformations all involve a reduction in the value of the atomic volume: from $V_{\text{fcc}}^{\text{initial}} = 7.01 \text{ \AA}^3$, $V_{\text{hcp}}^{\text{initial}} = 6.67 \text{ \AA}^3$, and $V_{\text{bcc}}^{\text{initial}} = 6.63 \text{ \AA}^3$ to $V_{\text{cd}}^{\text{final}} = 5.65 \text{ \AA}^3$. A kinetic energy cutoff of

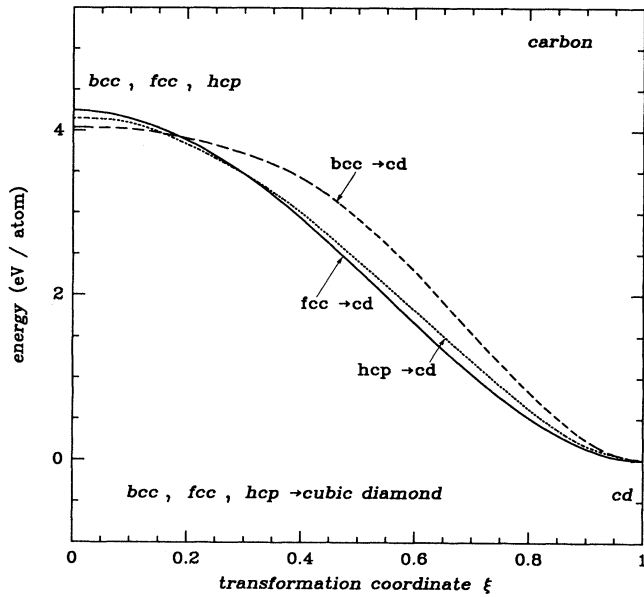


FIG. 8. Calculated total energy per atom as a function of the parameter ξ describing fcc \rightarrow cd (solid line) and hcp \rightarrow cd (dotted line) transformations, using the 4c sites of space group $Pnma$, and a bcc \rightarrow cd (dashed line) transformation, using the 2c sites of space group $R\bar{3}m$. Throughout the transformations, the structures are described by a primitive cell with a 4-atom basis for the fcc \rightarrow cd and hcp \rightarrow cd transformations and a 2-atom basis for the bcc \rightarrow cd transformation. The atomic volume varies along the transformation path: The initial and final atomic volumes are $V_{\text{fcc}}^{\text{initial}} = 7.01 \text{ \AA}^3$, $V_{\text{hcp}}^{\text{initial}} = 6.67 \text{ \AA}^3$, $V_{\text{bcc}}^{\text{initial}} = 6.63 \text{ \AA}^3$, and $V_{\text{cd}}^{\text{final}} = 5.65 \text{ \AA}^3$. A kinetic energy cutoff of $E_{\text{cutoff}} = 45 \text{ Ry}$ was used for all the calculations. The number of special \mathbf{k} points used was 27 for the fcc \rightarrow cd, 27 for the hcp \rightarrow cd and 28 for the bcc \rightarrow cd. The zero of energy corresponds to the (cubic or hexagonal) diamond structure.

TABLE IV. $R\bar{3}$ (C_{3i}^2 , No. 148) paths from bc8 to cubic diamond (cd) and rhombohedral graphite (rg). The $R\bar{3}$ conventional cell is rhombohedral, i.e., edge lengths $a = b = c$ and angles $\alpha = \beta = \gamma$, where α is the angle between \mathbf{b} and \mathbf{c} . The relations between the $R\bar{3}$ parameters and the usual cubic (a_{bc8} , $x_{\text{bc8}} \approx 0.1$, a_{cd}) or rhombohedral (a_{rg} , $\alpha_{\text{rg}} = 39.5^\circ$) quantities are shown, as well as the corresponding $p = 0$ values a_0 of a . The dimensionless parameters x_1 define 2c sites $[\pm(x, x, x)]$, while x_2 , y_2 , and z_2 define 6f sites $[\pm(x, y, z), \pm(z, x, y), \pm(y, z, x)]$.

$R\bar{3}$	bc8	cd	rg
a	$a_{\text{bc8}} \sqrt{3}/2$	a_{cd}	$a_{\text{rg}} \sqrt{3 - 2 \cos \alpha_{\text{rg}}}$
a_0 (\AA)	3.83	3.57	4.40
$\cos \alpha$	$-\frac{1}{3}$	0	$-1 + 2/(3 - 2 \cos \alpha_{\text{rg}})$
α	109.5°	90°	68.1°
x_1	$2x_{\text{bc8}}$	$\frac{1}{8}$	$\frac{1}{6}$
x_2	$2x_{\text{bc8}} + \frac{1}{2}$	$\frac{5}{8}$	$\frac{2}{3}$
y_2	$\frac{1}{2}$	$\frac{5}{8}$	$\frac{2}{3}$
z_2	0	$\frac{1}{8}$	$\frac{1}{6}$

$E_{\text{cutoff}} = 45 \text{ Ry}$ was used for all the calculations. The number of special \mathbf{k} points used was 27 for the fcc \rightarrow cd, 27 for the hcp \rightarrow cd, and 28 for the bcc \rightarrow cd.

Inspection of Fig. 8 reveals that the fcc, hcp, and bcc high-coordination metallic phases of carbon are mechanically unstable at atmospheric pressure against a transformation to a low-energy cubic diamond phase. This result is in agreement with previous theoretical results which have demonstrated a similar mechanical instabil-

TABLE V. $C2/c$ (C_{2h}^6 , No. 15) paths from bc8 to orthorhombic (og, see Ref. 22) and rhombohedral (rg) graphite. This monoclinic distortion (angle β between \mathbf{a} and \mathbf{c} different from 90°) of the bc8 \rightarrow og path in Table I permits sliding of the graphitic layers over one another toward an rg final state. The relations between the $C2/c$ parameters and the usual cubic (a_{bc8} , $x_{\text{bc8}} \approx 0.1$), hexagonal (a_{hg} , c_{hg}), and rhombohedral (a_{rg} , $\alpha_{\text{rg}} = 39.5^\circ$) quantities are shown. The dimensionless parameters x_1 , y_1 , and z_1 define one set of 8f sites; and x_2 , y_2 , and z_2 , another. The 8f sites ($I12/a1$ setting/cell choice) are $\pm(x, y, z)$ and $\pm(\bar{x} + \frac{1}{2}, y, \bar{z})$, plus the same added to $(\frac{1}{2}, \frac{1}{2}, \frac{1}{2})$.

	bc8	og	rg
a	a_{bc8}	$\sqrt{3} a_{\text{hg}}$	$\sqrt{6(1 - \cos \alpha_{\text{rg}})} a_{\text{rg}}$
b	a_{bc8}	$2 a_{\text{hg}}$	$\sqrt{8(1 - \cos \alpha_{\text{rg}})} a_{\text{rg}}$
c	a_{bc8}	c_{hg}	$\sqrt{3(1 + 2 \cos \alpha_{\text{rg}})} a_{\text{rg}}$
$\cos \beta$	0	0	$\left[3 \left(\frac{1 - \cos \alpha_{\text{rg}}}{1 + \cos \alpha_{\text{rg}}} \right) \right]^{1/2}$
x_1	x_{bc8}	$\frac{1}{12}$	$\frac{1}{12}$
y_1	x_{bc8}	$\frac{1}{8}$	$\frac{1}{8}$
z_1	x_{bc8}	0	0
x_2	x_{bc8}	$\frac{1}{12}$	$\frac{1}{12}$
y_2	$\frac{1}{2} + x_{\text{bc8}}$	$\frac{5}{8}$	$\frac{5}{8}$
z_2	$-x_{\text{bc8}}$	0	0

TABLE VI. $Pnma$ (D_{2h}^{16} , No. 62) paths to cubic diamond (cd) from face-centered cubic (fcc), hexagonal close packed (hcp), and body-centered cubic (bcc) structures. The $Pnma$ conventional cell is primitive orthorhombic with edge lengths a , b , and c , whose relations to the various lattice constants are shown. The dimensionless parameters x and z specify the $4c$ sites given by $\pm(x, \frac{1}{4}, z)$ and $\pm(\bar{x} + \frac{1}{2}, \frac{3}{4}, z + \frac{1}{2})$. The number of fcc, hcp, or bcc near neighbors which evolve into near neighbors in the cd structure is given by n .

	fcc	hcp	bcc	cd
a	a_{fcc}	$\sqrt{3} a_{hcp}$	$\sqrt{2} a_{bcc}$	$a_{cd}/\sqrt{2}$
b	a_{fcc}	c_{hcp}	$\sqrt{2} a_{bcc}$	$a_{cd}/\sqrt{2}$
c	a_{fcc}	a_{hcp}	a_{bcc}	a_{cd}
x	$\frac{1}{4}$	$\frac{1}{3}$	$\frac{1}{4}$	$\frac{1}{2}$
z	0	0	0	$\frac{1}{8}$
n	4	4	2	—

ity for the $sc \rightarrow cd$ and $\beta\text{-Sn} \rightarrow cd$ transformations.¹² On the basis of these results, one might speculate that all high-coordination phases of carbon would exhibit mechanical instabilities at atmospheric pressure. They also suggest the unlikely occurrence of stable or metastable local structure with coordination number higher than four in liquid and amorphous carbon as well as in carbon clusters, unlike the situation for Si. *Ab initio* molecular dynamics simulations of liquid and amorphous carbon have recently confirmed these expectations.¹⁶

VI. SUMMARY

The stability of various energetic phases of carbon at atmospheric pressure has been investigated by the use of a space-group-theoretical analysis of possible transformation paths to lower-energy phases, combined with *ab initio* pseudopotential calculations of the total energy along these paths. In particular, we have examined the stability of the fourfold-coordinated bc8 phase of carbon, and identified natural, low-barrier decay channels to threefold-coordinated graphitic structures and to the hexagonal form of diamond. We find energy barriers along all of these paths, with the *smallest* encountered along nearly identical paths to an intermediate orthorhombic form of graphite and to the observed hexagonal form. A simple distortion of the first path leads to the observed rhombohedral form of graphite, although the required sliding motion of the incipient graphitic layers over one another is energetically unfavorable until the transformation to orthorhombic graphite is nearly complete. Our results suggest the existence of a barrier of *at least* ≈ 0.2 eV/atom inhibiting transformation of an atmospheric bc8 phase of carbon to all lower-energy graphitic and diamond phases. Consequently, it appears that the bc8 phase is likely to be mechanically stable at atmospheric pressure.

In contrast, we find three metallic high-coordination forms of carbon (face-centered cubic, hexagonal close-packed, and body-centered cubic) to be mechanically un-

TABLE VII. $R\bar{3}m$ (D_{3d}^5 , No. 166) paths to cubic diamond (cd) from face-centered cubic (fcc) and body-centered cubic (bcc). The $R\bar{3}m$ conventional cell is rhombohedral, i.e., edge lengths $a = b = c$ and angles $\alpha = \beta = \gamma$, where α is the angle between b and c . The relations between a and the usual lattice constants of the various structures is shown. The dimensionless parameter x specifies the $2c$ sites $\pm(x, x, x)$. The number of fcc or bcc near neighbors which evolve into near neighbors in the cd structure is given by n .

	fcc	bcc	cd
a	$\sqrt{3/2} a_{fcc}$	a_{bcc}	$a_{cd}/\sqrt{2}$
α	$\cos^{-1}(\frac{5}{6}) = 33.6^\circ$	90°	60°
x	$\frac{1}{4}$	$\frac{1}{4}$	$\frac{1}{8}$
n	3	4	—

stable against spontaneous transformation to the cubic diamond structure. This result reaffirms the general expectation that possible metastable phases of carbon at atmospheric pressure are likely to be three- or fourfold coordinated.

ACKNOWLEDGMENTS

The authors are indebted to K. Kunc, O. H. Nielsen, R. J. Needs, and R. M. Martin, whose pseudopotential plane-wave developments we have used. This work was supported by the Lawrence Livermore National Laboratory under Contract No. W-7405-ENG-48 to the U.S. Department of Energy, and in part under ARPA order 7431 of the A/A program.

APPENDIX

In this appendix we provide supplementary information about the transition paths discussed in Sec. II. Table IV gives the $R\bar{3}$ mappings from bc8 to cd and rg, which were listed in Table II. The $2c$ sites of higher symmetry $R\bar{3}m$ are a familiar path from cd to rg.¹⁷ The mapping in Table IV quadruples this cell by taking the rhombohedral angle for cd to be 90° rather than 60° .

Because of the importance of the bc8 \rightarrow og path given in Table I we provide a monoclinic distortion of this path in Table V. These $C2/c$ mappings permit lateral sliding of the graphiticlike layers over one another, at any stage of the transformation in Table I, and include the possibility of an rg final state.

Previous theoretical studies¹² have predicted that the sixfold coordinated β -tin and simple cubic phases of carbon would be mechanically unstable at atmospheric pressure, and speculated that all high-coordination structures would be similarly unstable. To test this possibility we provide transformation paths to cd from fcc, hcp, and bcc structures in Tables VI and VII. It seems intuitively clear that the most natural paths will be ones in which four of the near neighbors of these high-coordination structures evolve into the four near neighbors of cd. Thus we choose the $Pnma$ paths in Table VI for the fcc and hcp cases; and the $R\bar{3}m$ path in Table VII, for the bcc case.

- ¹J. C. Angus and C. C. Hayman, *Science* **241**, 913 (1988); W. A. Yarbrough and R. Messier, *ibid.* **247**, 688 (1990).
- ²N. N. Matyushenko, V. E. Strel'nitskii, and V. A. Gusev, *Pis'ma Zh. Eksp. Teor. Fiz.* **30**, 218 (1979) [*JETP Lett.* **30**, 199 (1979)]; A. S. Bakai and V. E. Strel'nitskii, *Zh. Tekh. Fiz.* **51**, 2414 (1981) [*Sov. Phys. Tech. Phys.* **26**, 1425 (1981)].
- ³R. L. Johnston and R. Hoffman, *J. Am. Chem. Soc.* **111**, 810 (1989).
- ⁴I. V. Stankevich, M. V. Nikerov, and D. A. Bochvar, *Usp. Khim.* **53**, 1101 (1984) [*Russ. Chem. Rev.* **53**, 640 (1984)]; I. V. Stankevich, M. V. Nikerov, E. G. Gal'pern, and D. A. Bochvar, *Zh. Strukt. Khim* **28**, 96 (1987) [*J. Struc. Chem.* **28**, 542 (1988)].
- ⁵K. M. Merz, Jr., R. Hoffmann, and A. T. Balaban, *J. Am. Chem. Soc.* **109**, 6742 (1987).
- ⁶M. A. Tamor and K. C. Hass, *J. Mater. Res.* **5**, 2273 (1990).
- ⁷A. Y. Liu, M. L. Cohen, K. C. Hass, and M. A. Tamor, *Phys. Rev. B* **43**, 6742 (1991).
- ⁸L. S. Palatnik, M. B. Guseva, V. G. Babaev, N. F. Savchenko, and I. I. Fal'ko, *Zh. Eksp. Teor. Fiz.* **87**, 914 (1984) [*Sov. Phys. JETP* **60**, 520 (1984)]; N. F. Savchenko, M. B. Guseva, V. G. Babaev, and L. S. Palatnik, *Phys. Chem. Mech. Surfaces* **4**, 1816 (1986).
- ⁹See, e.g., C. Zener, in *Phase Stability in Metals and Alloys*, edited by P. S. Rudman, J. Stringer, and R. I. Jaffee (McGraw-Hill, New York, 1966), p. 25.
- ¹⁰R. Biswas, R. M. Martin, R. J. Needs, and O. H. Nielsen, *Phys. Rev. B* **30**, 3210 (1984).
- ¹¹M. T. Yin, *Phys. Rev. B* **30**, 1773 (1984).
- ¹²S. Fahy and S. G. Louie, *Phys. Rev. B* **36**, 3373 (1987).
- ¹³J. Donohue, *The Structures of the Elements* (Wiley, New York, 1974).
- ¹⁴J. Z. Hu and I. L. Spain, *Solid State Commun.* **51**, 263 (1984).
- ¹⁵W. Krättschmer, L. D. Lamb, K. Fostiropoulos, and D. R. Huffman, *Nature (London)* **347**, 354 (1990).
- ¹⁶G. Galli, R. M. Martin, R. Car, and M. Parrinello, *Phys. Rev. Lett.* **62**, 555 (1989); *Phys. Rev. B* **42**, 7470 (1990).
- ¹⁷S. Fahy, S. G. Louie, and M. L. Cohen, *Phys. Rev. B* **34**, 1191 (1986); **35**, 7623 (1987).
- ¹⁸D. J. Erskine and W. J. Nellis, *Nature (London)* **349**, 317 (1991).
- ¹⁹F. P. Bundy, H. P. Bovenkerk, H. M. Strong, and R. H. Wentorf, Jr., *J. Chem. Phys.* **35**, 383 (1961).
- ²⁰*International Tables for Crystallography*, Vol. A, *Space-Group Symmetry*, edited by Theo Hahn, 2nd ed. (Kluwer Academic, Dordrecht, 1989).
- ²¹See Ref. 13. We assume the hexagonal layers in hexagonal graphite to be completely flat, i.e., we take the higher $P6_3/mmc$ symmetry, as discussed by Donohue.
- ²²By orthorhombic graphite (og) we refer to the $8h$ sites of space group $Fmmm$ (D_{2h}^{23} , No. 69), where $y = \frac{1}{6}$ and $b/a = \sqrt{3}$. The structure is face-centered orthorhombic with a basis $\pm(0,y,0)$, and is illustrated in Fig. 1. Since it is not observed experimentally we describe og throughout this paper with reference to the more familiar lattice constants of hexagonal graphite (hg). In the $Fmmm$ representation, $a_{og} = a_{hg}$, $b_{og} = \sqrt{3} a_{hg}$, and $c_{og} = c_{hg}$.
- ²³See, for example, *Theory of the Inhomogeneous Electron Gas*, edited by S. Lundqvist and N. M. March (Plenum, New York, 1983).
- ²⁴J. Ihm, A. Zunger, and M. L. Cohen, *J. Phys. C* **12**, 4409 (1979).
- ²⁵D. R. Hamann, M. Schlüter, and C. Chiang, *Phys. Rev. Lett.* **43**, 1494 (1979).
- ²⁶G. B. Bachelet, D. R. Hamann, and M. Schlüter, *Phys. Rev. B* **26**, 4199 (1982).
- ²⁷D. M. Ceperley and B. J. Alder, *Phys. Rev. Lett.* **45**, 566 (1980).
- ²⁸O. H. Nielsen and R. M. Martin, *Phys. Rev. Lett.* **50**, 697 (1983); *Phys. Rev. B* **32**, 3780 (1985).
- ²⁹H. J. Monkhorst and J. D. Pack, *Phys. Rev. B* **13**, 5188 (1976).
- ³⁰O. H. Nielsen and R. M. Martin, *Phys. Rev. B* **32**, 3792 (1985).
- ³¹M. T. Yin and M. L. Cohen, *Phys. Rev. B* **26**, 5668 (1982).
- ³²The number of special k points used were 10 (cd), 12 (hd), 18 (bc8), 32 (og), 35 (sc), 26 (bcc), 36 (hcp), and 28 (fcc).
- ³³F. D. Murnaghan, *Proc. Natl. Acad. Sci.* **30**, 244 (1944).
- ³⁴The linearized bc8 \rightarrow hd (path 3, Table II) mapping needlessly compresses one bond, that indicated by the dotted curve in Fig. 2(b). This follows from the change in sign of $y_2 - \frac{1}{2}$ during the evolution from bc8 to hd, as is evident in Table I. A simple improvement is to maintain the direction of the vector $(x_2 - \frac{1}{2}, y_2 - \frac{1}{2}, z_2 - \frac{1}{2})$ as specified by the linear mapping; however, increase its magnitude to equal that of (x_1, y_1, z_1) . For such a path, the four nearest-neighbor distances are the same for the two inequivalent sites, and the barrier height $\Delta E_b(\text{bc8} \rightarrow \text{hd})$ is reduced from 0.54 to 0.38 eV/atom.
- ³⁵Y. Waseda and K. Suzuki, *Z. Phys. B* **20**, 339 (1975).
- ³⁶J. P. Gabathuler and S. Steeb, *Z. Naturforsch.* **34a**, 1314 (1979).
- ³⁷D. Tománek and M. A. Schlüter, *Phys. Rev. Lett.* **56**, 1055 (1986).
- ³⁸H. J. McSkimin and P. Andreatch, Jr., *J. Appl. Phys.* **43**, 985 (1972).